JOURNAL OF PROPULSION AND POWER
Vol. 21, No. 4, July–August 2005

Boundary-Layer Control in Mach 4 and Mach 6 Scramjet Engines

Tohru Mitani,* Noboru Sakuranaka,† Sadatake Tomioka,‡ and Kan Kobayashi§
Japan Aerospace Exploration Agency, Miyagi 981-1525, Japan

Boundary-layer ingestion in airframe-integrated scramjet engines causes engine stall (engine unstart hereafter) and restricts engine performance. To improve the unstart characteristics in engines, boundary-layer bleed and a two-staged injection of fuel were examined in Mach 4 and Mach 6 engines. The bleed system consisting of a porous plate, an air cooler, a metering orifice, and an on/off valve was designed for each of the engines. First, a method to determine bleed rates was developed. Porous plates were designed to extract air from the Mach 4 engine at a rate of 200-g/s and from the Mach 6 engine at a rate of 30 g/s. Air coolers were then optimized based on the bleed rates. The exhaust air could be cooled below 600 K in the porous plates and the compact air coolers. The Mach 4 engine tests showed that the 200-g/s bleed (3% of the captured air) doubled an engine operating range (limit fuel rate) and thrust. With two-staged injection of H_2, the engine operating range was extended from Φ0.3 to Φ0.95, and the maximum thrust was increased from 1200 to 2560 N. The Mach 6 tests showed that the 30-g/s bleed (0.6% of the captured air) extended the start limit from Φ0.48 to Φ1 and increased the maximum thrust from 1620 to 2460 N.

Nomenclature

C_d = flow discharge coefficients in bleed-plate holes
c_f = wall friction coefficient in Eq. (2)
D_{int} = internal drag of engines (measured by subscale wind tunnels)
d_1 = displacement thickness of boundary layer swallowed by engines
F_{net} = net thrust, $\Delta F - D_{\text{int}}$
I_{sp} = fuel specific impulse, F_{net}/fuel mass flow rate, km/s
M = Mach number
Ma = air mass flow rate captured by engines (measured by subscale wind tunnels), Mach 4 condition, Mach 6 condition
P_0 = total pressure, 0.9 MPa at Mach 4 and 4.5 MPa at Mach 6 conditions
P_1 = static pressure at the exit of inlet in Eq. (2)
P_2 = static pressure raised by combustion in Eq. (2)
x = streamwise distance in engine measured from the leading edge
ΔF = thrust increment by combustion (measured by a force balance in engine wind tunnels)
ε = geometrical contraction ratio of inlets
η_c = air capture ratio in engines (measured by subscale wind tunnels)
η_{P2} = total pressure recovery factor at the entrance of combustor (measured by subscale wind tunnels)
Φ = H_2 equivalence ratio

Subscripts

exp = experimental
1D = one-dimensional analysis

Received 31 January 2004; revision received 14 September 2004; accepted for publication 5 January 2005.

*Group Leader, Combined Propulsion Research Group, Kakuda Space Propulsion Center, Kimigaya, Kakuda; mitani.tohru@jaxa.jp.
†Senior Researcher, Combustion Laboratory, Combined Propulsion Research Group, Kakuda Space Propulsion Center, Kimigaya, Kakuda.
‡Laboratory Leader, Combustion Laboratory, Combined Propulsion Research Group, Kakuda Space Propulsion Center, Kimigaya, Kakuda. Member AIAA.
§Researcher, Combustion Laboratory, Combined Propulsion Research Group, Kakuda Space Propulsion Center, Kimigaya, Kakuda. Member AIAA.

Introduction

AIRFRAME-INTEGRATED scramjet engines swallow the boundary layer developed on airframes of space planes. This ingestion promotes boundary-layer separation in the engine and causes engine stall in combustion tests (engine unstart in this paper) because of loss of thrust. As a result, maximum fuel supply rates and thrust are limited. Tests of H_2-fueled scramjet engines have shown previously that the limit equivalence ratios Φ^* at the engine unstart were 0.3 at Mach 4 and about 0.5 at Mach 6 and 8 flight conditions.[1] Φ^* was greatly changed by exclusion of the boundary layers, in which the engine was moved into the nozzle core region.[2] For instance, the engine operation limit was extended from $\Phi^* = 0.42$ to $\Phi^* = 2.1$ and the thrust was increased from 316 to 1220 N by boundary-layer exclusion in Mach 8 tests. In scramjet engines, however, the exclusion of the boundary-layer by diverters is unrealistic because of severe aerodynamic heating and large installation drag.

Therefore, other methods for suppressing boundary-layer separation are required. Methods of boundary-layer control in subsonic flows are well summarized in Ref. 3. Some data on bleed-hole arrangements and discharge coefficients have been reported,[4–8] although there have been few reports on the effects of engine inlets, especially in supersonic engine performance.[9,10] Yanta et al.[9] conducted a wind-tunnel test with a bleed rate of 1.5% of the captured air in a Mach 4 ramp-compression inlet. Shimura et al.[10] reported the effect on engine-unstart prevention in one-fifth subscaled models of our scramjet engines. However, no quantitative discussion on prevention of engine unstart has been reported.

To improve the unstart characteristics in our engines, boundary-layer bleed and two-staged injection of fuel were examined in Mach 4 (Ref. 11) and Mach 6 (Ref. 12) engine tests. Figure 1 shows the engine used in those tests. Supersonic flow, accompanying the boundary layer, approaches the engine from the left. The thick boundary layer on the top wall of the engine (lower part in Fig. 1) is bled out through a porous plate. Two-staged injection is tested by adding a second fuel-orifice row downstream of the combustor. This distributed injection may moderate the pressure rise due to heat release in the combustor and, consequently, prevent engine unstart at higher fuel injection rates. Details of the engine test and results have been previously reported.[11–13] Those engine test data were compared with theoretical values and quantified as achievement factors.[14]

In this paper, details of the boundary-layer bleed are described, and the improvement of engine performance by bleed and two-stage injection is reviewed. A numerical simulation study has been completed against this Mach 6 engine test, in which the aerodynamic performance of the inlet, pressure distribution, thrust, and heat flux

Table 1 Test conditions and thrust performance measured in engine tests

Flow parameters	M_1	P_0, MPa	T_0, K	d_1, mm	ε	η_c	Ma, kg/s	M)H_2, g/s	Φ	ΔF_{exp}, N	D_{int}, N	F_{net}, N	I_{sp})f, km/s
Mach 4 without strut	3.4	0.86	870	11.7	2.86	0.72	6.70	195	0.30	1200	570	630	10.8
3% bleed	3.4	0.86	870	11.7	2.86	0.72	6.50	195	0.66	2300	700	1400	12.4
3% bleed and staged H2	3.4	0.86	870	11.7	2.86	0.72	6.50	195	0.95	2560	700	1860	10.0
Mach 6 with 5/5H-strut	5.3	4.8	1500	19.7	5.00	0.80	5.00	145	0.48	1620	780	840	12.0
0.6% bleed	5.3	4.8	1500	19.7	5.00	0.80	5.00	145	1.00	2460	780	1680	11.6

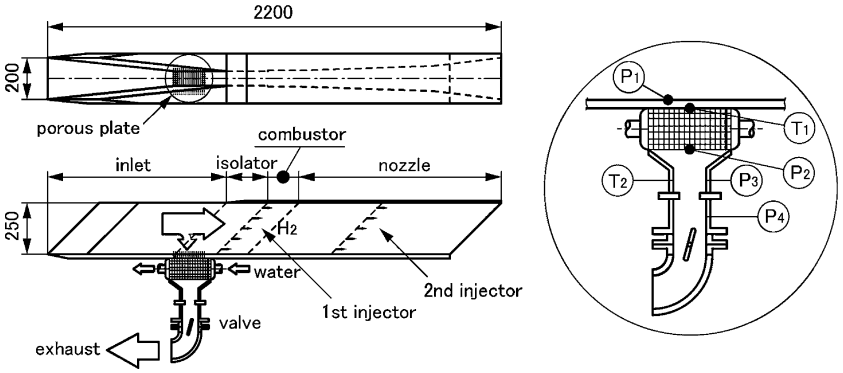

Fig. 1 Scramjet engine with boundary-layer bleed and two-staged injection of H_2.

on the engine walls are compared with engine data obtained in Mach 6 tests.[15] The computational results supported the improvement of engine performance by the boundary-layer control.

Engine Geometry, Test Conditions, and Thrust Measurement[1]

The side-compression-type engine shown in Fig. 1 is rectangular and consists of a cowl, a top wall, and two sidewalls. The entrance and the exit of the engine are 200 mm wide, 250 mm high, and 2.1 m long. The inlet has a wedge with a 6-deg half-angle and a swept-back angle of 45 deg to deflect the airstream for suitable spillage required in starting. The geometrical contraction ratio ε is 2.86 without struts for the M4 tests and a higher value of $\varepsilon = 5$ with installation of a 30-mm-thick strut for the M6 tests. Chinzei et al. reported the details of the engines, test methods, and accuracy of the engine testing.[1]

The test conditions and engine performances are summarized in Table 1, where the inlet Mach number M_1, the geometric contraction ratio ε, and the air capture ratio η_c are shown. The lower M_1, compared with the flight Mach numbers, represents the engine inlet condition behind the bow shock of vehicles. The 99% thickness of boundary layer is denoted by d_1 in Table 1. The d_1 was measured in calibration tests of the engine wind tunnel. The η_c was measured by using one-fifth subscale models and a choked flow meter in a subscale wind tunnels.[16,17]

In the M4 tests, the mass rate Ma (in kilograms per second) of air flowing in the inlet is 6.7 kg/s from the air capture ratio η_c. As shown in Table 1, the airflow rate in the combustor, however, decreases to 6.5 kg/s due to the boundary-layer bleed. The Ma with the strut is 5.0 kg/s with boundary-layer ingestion in the M6 condition. The bleed rate in the M6 test is so small that the Ma to the combustor is unchanged (5.0 kg/s).

Hydrogen (H_2) fuel was injected perpendicularly to the sidewalls from 12 sonic orifices (1.5 mm in diameter) located 30 mm downstream of backward-facing steps (4 mm high) in the combustor on each sidewall. The stoichiometric H_2 rate in Table 1 was determined by the airflow rates and found to be from 195 (M4 strutless engine) to 145 g/s (M6 engine with the 30-mm-thick strut). In some tests, two-staged injection of H_2 was examined to improve the thrust performance where the additional H_2 was injected 558-mm downstream of the combustor step.

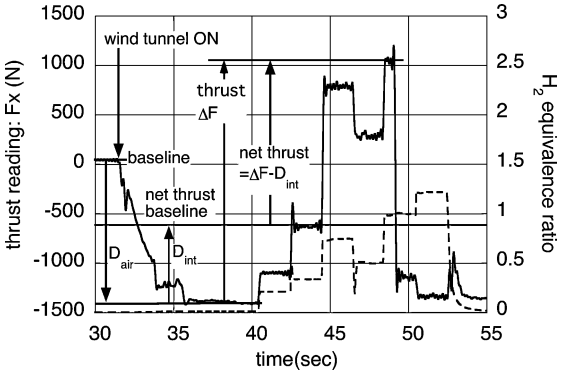

Fig. 2 Variations of thrust and H_2 supply rate and definitions of combustion thrust ΔF, internal drag D_{int}, and net thrust F_{net}.

Forces acting on engines were measured by a balance [force measuring system (FMS)] consisting of a floating frame supported by a thrust load cell (with the full range equal to 8.9 kN) and three load cells (22 kN) for lift and pitching moment. The FMS contains a calibration system driven by oil pressure and can revise the calibration matrix under conditions of installation of fuel and cooling water supply lines and measurement cables. This FMS measurement is a steady-state measurement in which test conditions are maintained from 2 to 10 s for each H_2 rate. Accuracy of the FMS was calibrated to be within $\pm 0.5\%$ in the thrust direction and within $\pm 1\%$ in the lift direction. The baselines of FMS before and after each wind-tunnel blowdown are compared to check baseline shifts sometimes caused by thermal stress in engines in the hot airflow.

Figure 2 shows a force measurement in a M6 test in which variations of thrusts (left-hand side) and H_2 equivalence ratio (right-hand side) are plotted. In Fig. 2, the M5.4 nozzle flow was established at 36 s. At first, engine drag D_{air} caused by airflow is measured without the fuel supply. The D_{air} is monitored before and after individual combustion sequences to examine the reproducibility of measurements. The air drag was measured to be 1340 N. Then the drag decreases, and thrust was produced stepwise due to engine combustion when the H_2 was supplied for 40.5 s. The H_2 rate was varied sequentially between $\Phi = 0.21$ and 1.22 (corresponding to H_2 flow rate of 177 g/s) in this experiment. The maximum thrust reading

was 1050 N at 49 s at $\Phi = 1$. Just after attaining maximum thrust, the engine fell to unstart, and the reading showed a drag of −1150 N with the same H_2 rate. This implies that the H_2 flow rate is the limit for engine operation. The unstart continued at $\Phi = 1.22$ till 52.5 s. A self-restarting of the engine, caused by the tailing off of fuel, is observed at 53 s. The engine test was completed at 53 s, and the D_{air} was measured at 55 s again to monitor drifts in the FMS readings.

The following performance properties are defined using Fig. 2. Combustion performance is indicated by a thrust increment measured from the D_{air}, and the increment is termed thrust by combustion or simply thrust ΔF here. Because $D_{\text{air}} = 1340$ N, the maximum thrust was found to be 2460 N at $\Phi = 1$ at 49 s. The D_{air} consists of two drags, namely, internal drags D_{int}, which worked on the internal walls in the engines, and external drags on the external surfaces. The external drag depends on the external geometry and decreases when engine modules are clustered. On the other hand, the D_{int} is related to irreversible processes, such as spill drag, total pressure loss in inlets, and friction loss in engines, and it is the most important and intrinsic property for evaluating engine performance. Therefore, net thrust is defined as $\Delta F - D_{\text{int}}$. Because D_{int} of the engine in Fig. 2 was 780 N, the maximum thrust was measured to be 1680 N.

However, the FMS readings contain drag produced on external surface of engines and drag on support rig of engines in wind-tunnel tests. Therefore, the ΔF was also evaluated by integration of wall pressure distributions to examine the accuracy of ΔF measured by FMS. Their correlation is shown in Fig. 3. The data symbols denote different test conditions, for instance, 1bld implies that H_2 was injected from 1 port 1 with boundary-layer bleed.

Accuracy in the FMS is within ±0.5%, and that in wall pressure measurement is within ±0.3%. The overall error bars in our measurements are much smaller than the symbols in Fig. 3. The most dominant source of errors in engine tests was repeatability in wall pressure $P_w(t)$ and $F_x(t)$ in Fig. 2. The overall errors, including the repeatability, were estimated be less than ±100 N in Fig. 3. Because increments of the friction drag due to combustion in the engines were 30 N in the M4 and 116 N in the M6 engines,[14] the good correlation between the two independent measurements in Fig. 3 evinces how reliable and accurate our thrust measurements are.

Design of Boundary-Layer Bleed Systems

Bleed Rates to Prevent Engine Unstart

Because measurements of the boundary layer are difficult in engine tests, we estimated its development in engines by numerical simulations.[15] Our computational fluid dynamics (CFD) studies showed that the momentum thickness of the boundary layer δ_2, on the top wall increased from 2.92 mm at the leading edge of inlet to 5.46 mm at the entrance of the combustor. A thinner δ_2 was found on the cowl and the sidewall (0.5 mm). Therefore, we installed the bleed section on the top wall.

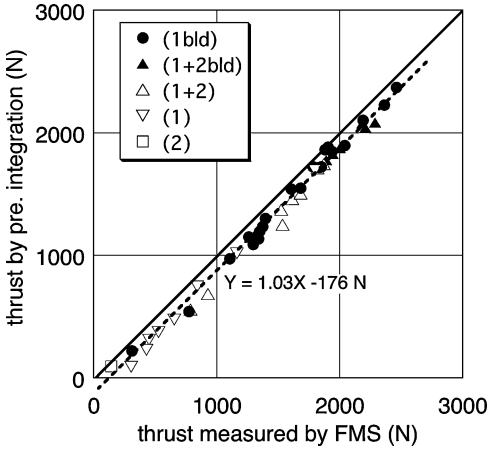

Fig. 3 Correlation between combustion thrust ΔF by FMS and by wall pressure integration.

The bleed rates to suppress boundary-layer separation were determined by a simplified boundary-layer consideration. Figure 4 shows maximum pressure rises observed in engine tests under M4 to M8 conditions, where P_1 is pressure at the entrance of isolator without combustion and P_2 is the maximum pressure just before unstart due to combustion. The engines fell into unstart condition when the pressure in the isolators exceeded the critical values. Because engine unstart is triggered by boundary-layer separation in the isolators, the critical pressure ratios must be correlated with Mach numbers there.

There are three lines in Fig. 4. The upper broken line denotes the thermal choke limit given by Eq. (1), where $\gamma (= 1.4)$ denotes the specific heat ratio. Comparison between the broken line and data indicates that engine unstart is not due to thermal choking but due to boundary-layer separation in the isolator. The line specified by Eq. (2) is the empirical limit of boundary-layer separation proposed by Holden,[18] where c_f is the wall friction coefficient. In our engine tests to date, data on critical pressure rises under engine combustion conditions have been accumulated. The data under conditions of boundary-layer ingestion are distributed around the line given by Eq. (3). In Eq. (3), a coefficient of 0.3 was proposed for two-dimensional separation by Korkegi.[19] However, Fig. 4 shows that a smaller value of 0.25 gives better correlation with three-dimensional separation data obtained in engine tests. Thus,

$$P_2/P_1 = (1 + \gamma M^2)/(1 + \gamma) \tag{1}$$

$$P_2/P_1 = 1 + 60 \cdot c_f \cdot M^3 \qquad \text{with} \qquad c_f = 0.002 \tag{2}$$

$$P_2/P_1 = 1 + 0.25 \cdot M^2 \tag{3}$$

Because the isolator Mach number can be calculated by one-dimensional analysis, the critical pressure rise $\Delta P (= P_2 - P_1)$ is obtained from Eq. (3). When a BL is subjected to ΔP, the separation can be prevented by removal of the bottom layer with local dynamic pressure lower than ΔP. Note that pressure rise assuming a normal shock wave yields no significant difference because the Mach number in the bottom layer is small. The ΔP showed that the critical Mach number in the bottom layer to be extracted was approximately $M^* = 1.6$ for the M4 and M6 engines. The one-seventh power law for velocity distribution in boundary layers yields bleed rates of 120 g/s (M4) and 130 g/s (M6). Devices were designed to target a bleed rate of 200 g/s in engine test conditions.

Figure 5 shows shock wave patterns and arrangements of the bleed plate, where the upper-half is for the M4 condition and the lower-half is for the M6 condition. The streamwise locations are measured from the leading edge of the sidewall. The exit of the inlet is located at $x = 617$ mm, and the backward-facing step in the combustor is located at $x = 817$ mm. A constant area section with a 70-mm-wide isolator is stationed at $617 < x < 817$ mm. The two circles in Fig. 5 just upstream of the step represent the torch ignitors in the M4 and M6 tests.

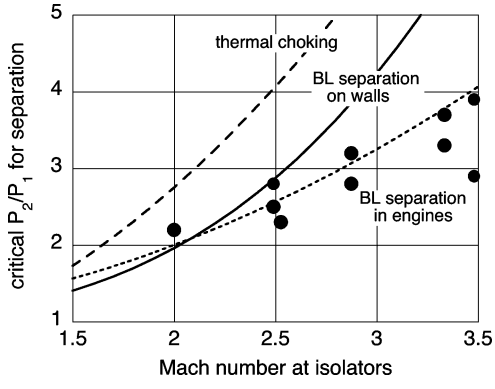

Fig. 4 Relations between critical adverse pressure ratios and Mach numbers in engine tests from M4 to 8.

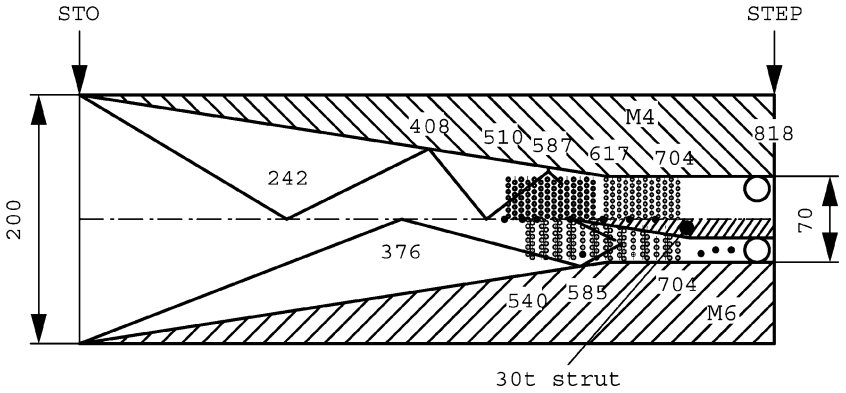

Fig. 5 Shock wave patterns and arrangements of porous plates for M4 and M6.

In the M4 condition, an oblique shock wave is generated at the leading edge of the sidewall, reflected back at the center ($x = 242$ mm), and impinges at $x = 408$ mm on the sidewall. The shock wave reflection raises the wall pressure near the exit of the inlet. Similarly, the shock wave in the M6 condition is reflected back at $x = 585$ mm on the sidewall, and another shock wave is generated at the leading edge of the strut ($x = 475$ mm). Thus, the region near the exit of the inlet suffers the most severe adverse pressure. Therefore, the starting points of bleed were chosen to be $x = 510$ mm for the M4 and 540 mm for the M6 engines to bleed the boundary layer developed in the inlet. The pressure rise due to combustion moves upstream from the combustor step located at $x = 817$ mm with increasing fuel rate. The terminal point of the porous plates was set at $x = 704$ mm to prevent boundary-layer separation by combustion.

As a result, the M4 bleed area was 5130 mm^2. The porous plate has 533 holes, 3.5 mm in diameter. (The total hole area/bleed area is the void ratio $= 0.385$.) Harloff and Smith[6] and Chyu et al.[7] found a small discharge coefficient C_d of about 0.2 for their bleed holes from their numerical analysis. However, a discharge coefficient was measured to be 0.51 under the inlet condition. Because of to the 30-mm-thick strut in the M6 engine, the bleed area was decreased to 2460 mm^2. A porous plate containing 196 holes with a diameter of 4 mm was designed for the small bleed area. The isolator pressure was also lower at 20 kPa in the M6 condition as compared with 40 kPa in the M4 case. Consequently, the maximum bleed rate in the M6 tests was reduced to 30 g/s as compared with 200 g/s in the M4 case.

Air Coolers and Exhaust

Hot air with total temperatures of 870 K (M4) and 1500 K (M6) required air coolers in the bleed systems. The air coolers were installed downstream of the porous plates as shown in Fig. 1. The bleed rates of 200 g/s and 30 g/s corresponded to 3% (M4) and 0.6% (M6) of the total airflow rates in engines, respectively. The small suction rates make the air cooler more compact for two reasons. First, the amounts of air to be cooled are small. Second, the temperature of the air bled is low because the bottom layer in boundary layer has already been cooled by the engine top wall. The coolers were designed to meet the requirement that the exhaust temperature should not exceed 650 K, even in the unstart condition.

The air bled through the porous plates is cooled in the plate. The M4 plate was uncooled, and the M6 plate was water cooled by 11 water passages. The air coolers were installed after the porous plates. A radiator for air conditioning in a compact car was utilized as the air cooler for the M4 bleed. Based on the hydraulic diameter of the finned-tube radiator (2.43 mm) and the air passage length (65 mm), it is estimated that the air temperature decreased by 0.3 times the initial difference in the temperature. The temperature of the exhaust from the cooler was estimated to be 480 K in the M4 condition. The M6 cooler (235 mm long, 95 mm wide, and 55 mm high) was made of small kettle boilers. It was estimated that a hydraulic diameter of 6.1 mm would lower air temperature by 400 K in the cooler. Because the bled air in the M6 tests was precooled in the water-cooled porous plate, it is estimated that the exhaust temperature was reduced lower than 600 K.

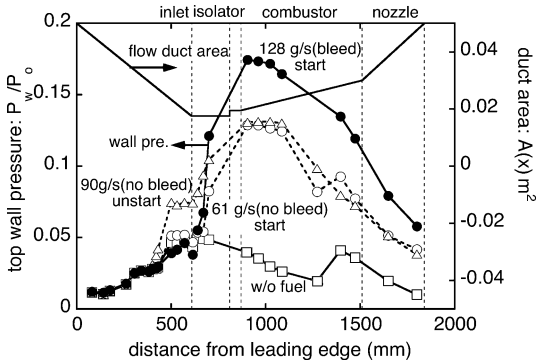

Fig. 6 Effects of boundary-layer bleed on wall pressure distributions, M4.

The static pressure in engines varies from 40 kPa (M4) to 20 kPa (M6). The bled air was autonomously exhausted to a test cell with a pressure of 12 kPa (M4) or 5 kPa (M6) after the bleed rates were metered with an orifice. ($C_d = 0.93$ by calibrations.) The bleed was controlled by an on/off valve during combustion tests. Pressure and air and water temperatures were monitored at locations indicated in Fig. 1.

Thrust Performance with Boundary-Layer Control

Mach 4 Tests

Figure 6 shows the effects of boundary-layer bleed on the wall pressure distributions on the top wall in the Mach 4 engines. The horizontal axis is the distance from the leading edge of the topwall. The wall pressure is normalized by the total pressure of the Mach 4 wind tunnel, $P_0 = 860$ kPa. The engine geometry is shown in the upper part of Fig. 6 where the inlet, the isolator, the backward-facing step, the diverging combustor, and the nozzle are indicated by broken lines.

The wall pressure distribution before fuel supply is indicated by open squares in Fig. 6. The pressure increases to $0.05P_0$ at the combustor due to compression in the inlet. The high-pressure air expands through the diverging sections ($x > 800$ mm) toward the nozzle. A fuel supply rate of 61 g/s (open circles) raises the wall pressure to $0.13P_0$ at the combustor, and this increase of the wall pressure in the diverging sections produces thrust. The high-pressure region is anchored in the isolator in the case of 61 g/s. However, an increase of fuel rate to 90 g/s causes intrusion of the high-pressure region into the inlet if boundary-layer bleed is not applied (open triangles). The intrusion of high-pressure region on the compression surface in the inlet increases drag and deteriorates thrust produced on the thrust surfaces. This is the engine unstart.

Effects of 200-g/s bleed are indicated by solid circles in Fig. 6. The bleed reduces pressure slightly on the porous plate around $x = 600$ mm. The most significant change is that the high-pressure region is stabilized in the isolator even with a larger fuel rate of 128 g/s. Because of this stabilization, the maximum pressure reaches $P = 0.175P_0$ and the higher pressure produces a greater thrust. Thus, the boundary-layer bleed is effective in anchoring the high-pressure region in the isolator and in suppressing engine unstart.

Figure 7 shows the effects of boundary-layer control on thrust increment ΔF by combustion in the Mach 4 engine. The open symbols in Fig. 7 denote data obtained in the engine without bleed, and the solid symbols are for the engine with boundary-layer bleed. The solid line (ΔF_{1D}) denotes the theoretically maximum ΔF where complete combustion and isentropic expansion of combustion gas are assumed in diverging sections of engines.[14] Because ΔF_{1D} is governed by airflow rate and total pressure at the entrance of combustors (location 2), η_c and η_2 were measured by using subscale engine models. Comparison of ΔF_{1D} with ΔF_{exp} can be related to bulk combustion efficiencies.[14]

In Fig. 7, the combustion mode switches from a weak mode (flame blown off to the downstream section) to an intense mode (flame anchored in the combustor), and the switch causes a jump in ΔF from 500 to 1000 N near $\Phi = 0.2$. The engine without bleed shows a peak ΔF of 1200 N at $\Phi = 0.3$, and the ΔF gradually diminishes in the region of $\Phi > 0.3$. This diminished ΔF_{exp} is caused by the intrusion of high-pressure region into the inlet as shown in Fig. 6. Because the internal drag D_{int} of the baseline engine was 570 N, the ΔF_{net} is 630 N and the I_{sp} is 10.8 km/s in Table 1.

Improved thrust performance with 200-g/s bleed (3% of the total airflow rate) is shown by the solid symbols in Fig. 7a. The engine operating range is now extended from $\Phi = 0.3$ to $\Phi = 0.66$, and the maximum ΔF doubles from 1200 to 2300 N. Engine internal drag on the internal wet surface of engines was precisely measured by using subscale aerodynamic wind tunnels,[16] and bleed drag was measured by our engine test procedure. The engine internal drag increased from $D_{int} = 570$ N without the bleed to 700 N with the bleed. Thus, the bleed drag was found to be 130 N in the engine. Results in Fig. 7a indicated that the engine net thrust increases from 630 to 1400 N with a 3% bleed. The corresponding fuel-specific impulse was 12.4 km/s at Φ0.66.

The secondary injection of H_2 from the downstream section of engine yields further improvement in the thrust performance, as shown in Fig. 7b. Because combustion due to the secondary fuel injection does not affect the flowfield in the isolator, the engine can operate from $\Phi = 0.66$ to $\Phi = 0.95$ and the maximum ΔF increases from 2300 to 2560 N. Consequently, F_{net} becomes 1860 N and the I_{sp} is found to be 10 km/s at $\Phi = 0.95$, as shown in Table 1.

Mach 6 Tests

Performance of the air cooler used in the Mach 6 engine is detailed in Fig. 8, where Fig. 8a shows pressure variations and Fig. 8b shows temperature histories. In Fig. 8a, the Mach 6 wind tunnel is activated at 32 s. Mach 6 steady flow is established at 35 s, and the engine test is commenced. Because hot air with a total temperature of 1500 K fills the cavity in the bleed system, the temperature upstream of the air cooler (behind the porous plate) increases gradually from 34 as shown in Fig. 8b. The boundary-layer bleed from 37 s decreases the pressure downstream of the measuring orifice to the test cell pressure (4 kPa). The sensor upstream of the orifice indicates 12 kPa. The bleed rate was measured by the pressure. Because of the hot air passing through the porous plate, the temperatures upstream and downstream of the cooler increase toward 550 and 350 K, respectively. The saturated temperature found downstream of the cooler implies that the cooling performance is sufficient in the start condition.

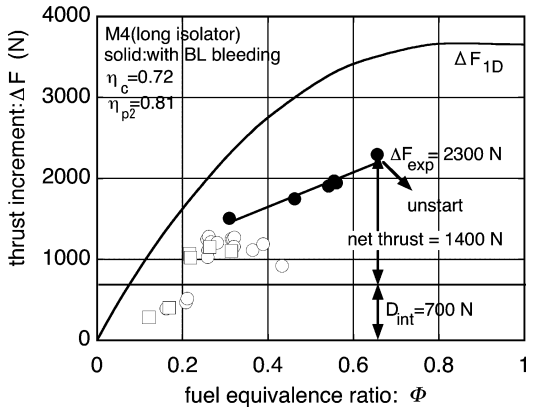

Fig. 7a Effect of boundary-layer bleed on thrust, M4.

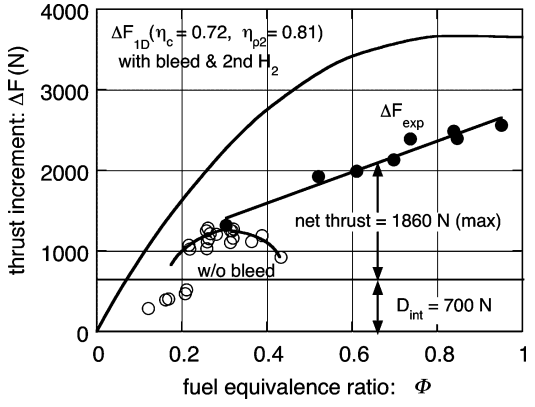

Fig. 7b Effect of boundary-layer bleed and and two-staged combustion, M4 long isolator.

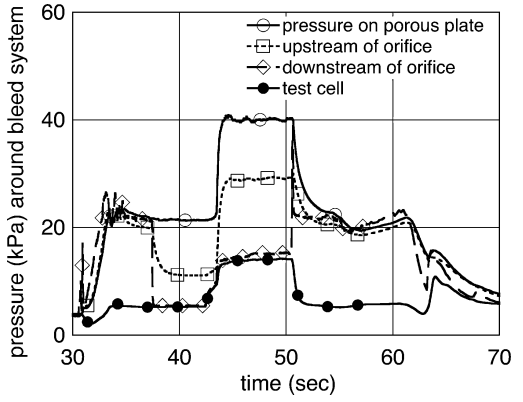

Fig. 8a Static pressure around the air cooler in the Mach 6 engine.

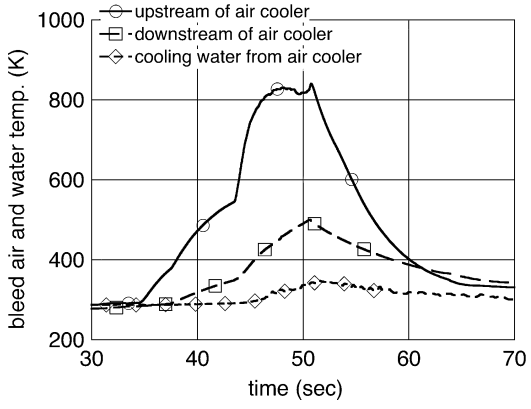

Fig. 8b Air and water temperature in the air cooler.

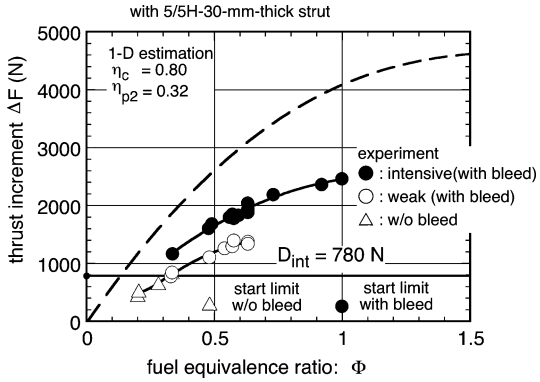

Fig. 9 Effect of boundary-layer bleed on thrust at M6.

With increasing H_2 injection rate, the engine falls into the unstart condition at 42 s and the condition continues until 51 s. This unstart causes engine-test facility interference and results in a pressure rise around the bleed system, as well as an increase in test cell pressure from 4 to 14 kPa. The gas temperature downstream of the cooler increases to 550 K, and the temperature upstream of the cooler is saturated at 800 K. These results indicate that the cooler functions well in the unstart condition. The engine restarts at 51 s and the engine test is conducted till $t = 60$ s. The maximum increase of cooling water temperature was found to be 50 K, and heat balance between the cooled air and the heated water was confirmed.

The test data at the Mach 6 condition are shown in Fig. 9. In these experiments, a 30-mm-thick strut is installed in the engine. The combustion mode switches from the weak mode to the intense mode, and the thrust jumps near $\Phi = 0.3$. Above $\Phi = 0.3$, the engine operates in the intense combustion mode. When the boundary layer is not bled, the engine falls into unstart at $\Phi = 0.48$ just after attaining the maximum thrust of 1620 N (shown by the open triangle in Fig. 9). Thus, the limit fuel rate is found to be $\Phi = 0.48$ without the bleed.

In Fig. 9, a bleed of 30 g/s (0.6% of captured air in the engine) extends the start limit from $\Phi = 0.48$ to $\Phi = 1$ to deliver a maximum thrust of 2460 N. The small bleed did not produce measurable bleed drag, and the D_{int} was found to be 784 N in the engine. When the D_{int} of 780 N, is subtracted, the F_{net} is 1680 N and the fuel I_{sp} is calculated to be 11.6 km/s as shown Table 1. This doubled thrust performance was reproduced by our numerical simulations, and the internal flowfield with combustion was investigated in detail.[15]

In the Mach 4 tests, the two-staged injection of H_2 extended the engine start limit and increased the maximum thrust. However, it did not improve the thrust performance in the Mach 6 condition. This is attributed to limited residence time of fuel in the engine. Because the second injectors are located 462 mm upstream of the engine exit, the residence time of fuel injected from the second injectors is insufficient for the mixing and combustion. Further studies on optimum injector locations in the multistaged combustors for scramjet engines are required.

Conclusions

A boundary-layer bleed system consisting of a porous plate, an air cooler, metering orifices, and an on/off valve was designed for each of the Mach 4 and Mach 6 engines. The bleed system was found to be effective in suppressing engine unstart transition. The following results were obtained in engine tests under Mach 4 and Mach 6 conditions.

1) Bleed rates for suppressing boundary-layer separation were analytically evaluated by comparing the local dynamic pressure in the bottom layer and the critical adverse pressure to induce engine unstart.

2) Air coolers were optimized based on the bleed airflow rates. The exhaust air could be cooled below 600 K by using the porous plates and compact air coolers.

3) Mach 4 engine tests showed that a small bleed rate of 3% doubled the engine operating range and the thrust at the $M4$ flight condition. With two-staged injection of H_2, the engine operating range was extended to $\Phi = 0.95$ and the maximum ΔF was improved from 2300 to 2560 N.

4) Mach 6 tests showed that a bleed of 30 g/s (0.6% of captured air in the engine) extended the start limit from $\Phi = 0.48$ to $\Phi = 1$, resulting in delivery of a maximum thrust of 2460 N. However, the two-staged injection of fuel did not improve the thrust performance in the $M6$ condition because the residence time of fuel injected from the second injectors was insufficient for mixing and combustion.

References

[1]Chinzei, N., Mitani, T., and Yatsuyanagi, Y., "Scramjet Engine Research at the National Aerospace Laboratory in Japan," *Scramjet Propulsion*, edited by E. T. Curran and S. N. B. Murthy, Vol. 189, Progress in Astronautics and Aeronautics, AIAA, Reston, VA, 2001, pp. 159–222.

[2]Hiraiwa, T., Kanda, T., Kodera, M., Saito, T., Kobayashi, K., and Kato, T., "Effect of Induced Boundary-Layer on Scramjet Engines' Thrust and Combustion Characteristics," AIAA Paper 2003-4739, July, 2003.

[3]Lachmann, G.,V. (ed.), *Boundary-Layer and Flow Control*, Vols. 1 and 2, Pergaman Press, New York, 1961.

[4]Fukuda, M. K., Hingst, W. R., and Eshotko, E., "Bleed Effects on Shock/Boundary-Layer Interactions in Supersonice Mixed Compression Inlets," *Journal of Aircraft*, Vol. 14, No. 2, 1977, pp. 151–156.

[5]Syberg, J., and Koncsek, J. L., "Bleed System Design Technology for Supersonic Inlets," *Journal of Aircraft*, Vol. 10, No. 7, 1973, pp. 407–413.

[6]Harloff, G. J., and Smith, G. E., "On Supersonic-Inlet Boundary-Layer Bleed Flow," AIAA Paper 95-0038, Jan. 1995.

[7]Chyu, W. J., "Effects of Bleed-Hole Geometry and Plenum Pressure on Three-dimensional Shock-Wave/Boundary-Layer/Bleed Interactions," AIAA Paper 93-3259, July 1993.

[8]Willis, B. P., Davis, D. O., and Hingst, W. R., "Flow Coefficient Behavior for Boundary-Layer Bleed Holes and Slots," AIAA Paper 95-0031, Jan. 1995.

[9]Yanta, W. J., Collier, A. S., Spring, W. C., III, Boyd, C. F., and McArthor, J. C., "Experimental Measurements of the Flow in a Scramjet Inlet at Mach 4," *Journal of Propulsion and Power*, Vol. 6, No. 6, 1990, pp. 784–790.

[10]Shimura, T., Izumikawa, M., Sakuranaka, N., Tomioka, S., and Watanabe, S., "M8 Simulation Tests on the Unstart Limit of a Scramjet Engine," International Symposium on Space Science and Technology, ISTS 02-A-17, June 2002.

[11]Kobayashi, K., Tomioka, S., Hiraiwa, T., Kato, K., Kanda, T., and Mitani, T., "Suppression of Combustor–Inlet Interaction in a Scramjet Engine under M4 Flight Condition," AIAA Paper 2003-4737, July 2003.

[12]Kodera, M., Tomioka, S., Kanda, T., and Mitani, T., "Mach 6 Test of a Scramjet Engine with Boundary-Layer Bleeding and Two-Staged Fuel Injection," AIAA Paper 2003-7049, Dec. 2003.

[13]Mitani, T., Sakuranaka, N., Tomioka, S., Kobayashi, K., and Kanda, T., "Doubled Thrust by Boundary-Layer Control in Scramjet Engines in Mach 4 and 6," Asian Joint Confs. on Propulsion and Power, March 2004.

[14]Mitani, T., Tomioka, S., Kanda, T., Chinzei, N., and Kouchi, T., "Scramjet Performance Achieved in Engine Tests from M4 to M8 Flight Conditions," AIAA Paper 2003-7009, Dec. 2003.

[15]Kouchi, T., Mitani, T., Kodera, M., and Masuya, G., "Numerical Experiments of Scramjet Combustion with Boundary-Layer Bleeding," AIAA Paper 2003-7038, Dec. 2003.

[16]Mitani, T., Izumikawa, M., Watanabe, S., and Tarukawa, Y., "Force Measurements of Fixied Geometry Scramjet Engines from Mach 4 to 8 Flight Condition," AIAA Paper 2002-5351, Sept. 2002.

[17]Kitamura, E., Mitani, T., Sakuranaka, N., and Masuya, G., "Evaluating the Aerodynamic Performance of Scramjet Engines by Pressure Measurement," AIAA 2003-7053, Dec. 2003.

[18]Holden, M. S., Shock Wave–Turbulent Boundary-Layer Interaction in Hypersonic Flow," AIAA Paper 72-0074, Jan. 1972.

[19]Korkegi, R. H., "A Lower Bound for Three-Dimensional Turbulent Separation in Supersonic Flow," AIAA *Journal*, Vol. 23, No. 3, 1985, pp. 475–476.